# Electric-field gradients at the Zr sites in Zr₃Fe: Measured using perturbed-angular-correlation spectroscopy and calculated using band theory

Arthur T. Motta, Stephen E. Cumblidge, and Gary L. Catchen

*Department of Mechanical and Nuclear Engineering, The Pennsylvania State University, University Park, Pennsylvania 16802*

Sergio B. Legoas

*Instituto de Física, Universidade Estadual de Campinas, Campinas, São Paulo, Brazil*

Andrea Paesano, Jr.

*Departamento de Física, Universidade Estadual de Maringá, Maringá, Paraná, Brazil*

Livio Amaral

*Instituto de Física, Universidade Federal do Rio Grande do Sul, Porto Alegre, Rio Grande do Sul, Brazil*

We have measured the electric-field-gradient (EFG) parameters $V_{ZZ}$ and $\eta$ and their temperature dependences at the two Zr sites in the intermetallic compound Zr₃Fe using perturbed-angular-correlation spectroscopy and the probe $^{181}$Hf$\rightarrow$$^{181}$Ta. At temperatures below the peritectic transformation at $\approx$1158 K, at each Zr site, we observed well-defined EFG's, characterized by sharp spectral lines. A high-frequency, very asymmetric nuclear electric-quadrupole interaction characterizes the first Zr site, which represents approximately one-third of the probes. A low-frequency, nearly axially symmetric nuclear electric-quadrupole interaction characterizes the second Zr site, which represents approximately two-thirds of the probes. Near and above the peritectic transformation, the results show the effects of the decomposition of Zr₃Fe into Zr and Zr₂Fe and subsequent melting. We have compared the values of $V_{ZZ}$ and $\eta$ measured at laboratory temperature to those calculated using the first-principles, self-consistent real-space linear muffin-tin atomic sphere approximation (RS-LMTO-ASA) band-theory method. Overall the magnitudes of $V_{ZZ}$ and $\eta$ calculated using the RS-LMTO-ASA method agree reasonably well with the experimental values.

## INTRODUCTION

In contrast to ordinary alloys, binary intermetallic compounds, such as Zr₃Fe, consist of crystals that have two distinct sublattices, and thus these compounds exhibit long-range chemical order. The atomic-scale environments around the atoms occupying these sublattices often differ significantly, because these structures usually have low symmetry. A consequence of the long-range order and the low symmetry is that the physical properties of these compounds are very sensitive to the presence of defects and dopants and deviations from stoichiometry. Moreover, these features (of long-range order and low symmetry) make intermetallic compounds good systems in which to investigate the kinetics and thermodynamics of defects and physical properties such as magnetic ordering and phase equilibria.

In addition to being important as model systems in these areas of fundamental physics, the Zr-Fe intermetallics have technological importance, because they can be used as hydrogen storage materials[1] and because they appear as second-phase particles in Zircaloy nuclear fuel cladding.[2] The stability of these second-phase particles affects the in-reactor behavior of the alloy. To understand the response of these phases to the effects of irradiation, it is necessary to understand the energy barriers associated with the transport of defects, which control the *in situ* annealing behavior of the material. Thus, to improve the technology associated with these intermetallics, we seek to better understand the physics of defects and the phase equilibria of these compounds.

## EXPERIMENTAL METHODS

To investigate the physics of defects and phase equilibria in these compounds, we use perturbed-angular-correlation (PAC) spectroscopy,[3] because with it we can observe local structural changes that accompany phase transformations via the nuclear electric-quadrupole interaction. In recent years, Collins and co-workers have investigated the thermodynamics of defects in a variety of intermetallic compounds,[4,5] and we have explored the effects of defects on magnetic ordering in ZrFe₂.[6] The PAC technique is based on substituting a relatively low concentration of a radioactive probe atom, in this case $^{181}$Hf$\rightarrow$$^{181}$Ta, into a well-defined site in a crystal. Because the chemistries of Hf and Zr are very similar, the probe $^{181}$Hf$\rightarrow$$^{181}$Ta substitutes into the Zr sites in Zr₃Fe. This probe can be added at relatively low levels, $\leqslant$0.1 at. % Hf, so that it does not measurably alter the global properties of the crystal.

Because of this sensitivity, PAC spectroscopy provides a unique means to investigate the nanometer-scale effects of local crystal fields at the Zr site in Zr₃Fe. Figure 1 presents a diagram of the orthorhombic Re₃B-type crystal structure of Zr₃Fe, which is stable from laboratory temperature to the peritectic temperature of approximately 1158 K.[7] The Zr₃Fe structure has two crystallographically distinct Zr sites. Because the nearest-neighbor environments around these two sites differ significantly, we measured the corresponding electric-field gradient (EFG's) to determine their temperature dependence and the corresponding changes that accompany a
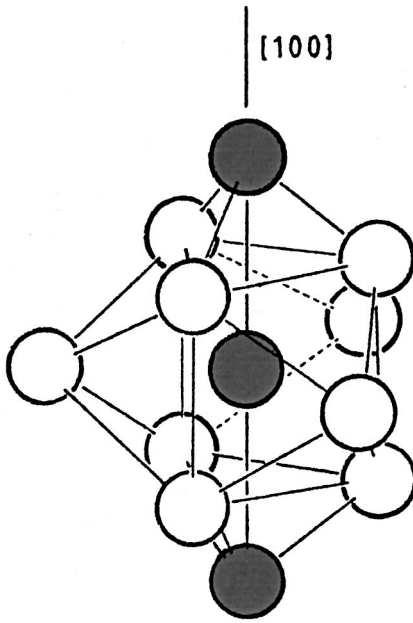
FIG. 1. The orthorhombic crystal structure of $Zr_3Fe$; Fe atoms are dark and Zr atoms are light (adapted from Ref. 7).

high-temperature transformation. Above the peritectic temperature, the $Zr_3Fe$ compound separates into two phases: the intermetallic compound $Zr_2Fe$ (which exhibits an $Al_2Cu$-type body-centered-tetragonal C16 structure) and hexagonal close-packed $\alpha$-Zr. Above 1200 K, this mixture melts eutectically to form a homogenous liquid phase.

We prepared samples of $(Zr_{1-x}Hf_x)_3Fe_{1+z}$ by arc-melting the pure constituents under an Ar atmosphere. The purities of the starting materials, obtained from Goodfellow Corporation, were 99.995% Fe and two Zr materials with different impurity contents: 99.8% Zr and 97% Zr (most of the impurity content in Zr consists of Hf and vice versa.) To produce the radioactive $^{181}$Hf isotope via the $^{180}$Hf$(n,\gamma)$ reaction, a small Hf wire was irradiated using the Penn State Breazeale Reactor. The Zr metal and radioactive Hf wire (containing both the radioactive $^{181}$Hf and $^{180}$Hf carriers) were first melted together to give a homogeneous Zr-Hf solid solution. This Zr-Hf mixture was then melted together with Fe metal. Each sample was melted 3 times to help achieve overall compositional homogeneity.

The resulting sample consisted of a mixture of phases, mostly hexagonal $\alpha$-Zr and body-centered-tetragonal $Zr_2Fe$. After melting, the sample showed negligible mass loss and had a bright, shiny appearance. After the sample cools from the melt and arrives at the peritectic temperature of 1158 K, the formation reaction of $Zr_3Fe$ (Zr+$Zr_2Fe \Rightarrow Zr_3Fe$) is very sluggish.[8] This kinetic constraint causes the two phases, stable at high temperature, to be observed normally after air cooling of the arc-melted sample. To transform the mixture of phases into the orthorhombic structure $[(Zr_{1-x},Hf_x)_3Fe_{1-z}]$ the sample was heated under vacuum at 1073 K for 96 h, at 1023 K for 72 h, and then at 1000 K for 48 h.[9] Two samples were prepared, one with $x=0.0024$ and $z=-0.003$ and one with $x=0.041$ and $z=-0.01$, which are well within the stoichiometry range reported for $Zr_3Fe$ of

23–27 at. % Fe ($-0.08<z<0.08$).[7] After the heat treatment, we confirmed that the radioactive samples consisted of a single phase using x-ray diffraction. The indexing was consistent with the $Re_3B$-type orthorhombic structure reported previously.[7,8,10] The samples were sealed in Ar-filled fused-silica tubes prior to performing the PAC measurements.

The PAC spectrometers are equipped with four ($BaF_2$ or CsF) scintillation detectors that give a nominal time resolution of 0.8–1.0 ns full width at half maximum for the $\gamma$ rays emitted in the decays of $^{181}$Hf. Samples were maintained at elevated temperatures using simple furnaces, which were controlled to $\pm2$ K. The perturbation functions $A_{22}G_{22}(t)$ measured below 1100 K were analyzed using a two-site model for static nuclear-electric-quadrupole interactions taking place in a polycrystalline sample:

$$-A_{22}G_{22}(t)$$

$$=\sum_{j=1}^{2} A_j\left[S_0+\sum_{k=1}^{3} S_k \exp(-\delta_j\omega_{jk}t)\cos(\omega_{jk}t)\right]+A_3.$$

$$(1)$$

Here $A_1$ and $A_2$ are the normalization factors, $\delta_1$ and $\delta_2$ are the Lorentzian line-shape factors that correspond to static line broadening, and $A_3$ takes into account both the effects of $\gamma$ rays that are absorbed in the sample en route to the detectors and the long-time behavior of the fraction of probe atoms that are not located in a well-defined chemical environment. The site-occupancy fractions are represented by $f_i = A_i/(A_1+A_2+A_3)$, $i=1,2$. The nonvanishing EFG components $V_{ii}$ in the principal-axis system where the probe nucleus is at the origin are related to the quadrupole frequency by $\omega_Q=eQV_{ZZ}/4I(2I-1)\hbar$, in which $Q$ represents the electric-quadrupole moment (2.51 b) for the $^{181}$Ta spin $I=(5/2)$ intermediate level. The perturbation functions measured above 1100 K were analyzed using phenomenological expressions based on Eq. (1).

## RESULTS AND DISCUSSION

Figure 2 shows the perturbation functions and the corresponding Fourier transforms for a $Zr_3Fe$ sample, measured at temperatures ranging from laboratory temperature to just below the peritectic transformation temperature, $T_p=1158$ K, at which $Zr_3Fe$ transforms into $\alpha$-Zr plus body-centered-tetragonal $Zr_2Fe$. These perturbation functions show relatively sharp line shapes, and for the perturbation functions measured from 298 to 1100 K, a two-site model, Eq. (1), provides an accurate representation of the measurements, and for the perturbation function measured at 1150 K, a three-site model provides an accurate representation of the measurement.

For the perturbation functions measured at 298 and 700 K, the Fourier transforms show three narrow peaks, which correspond to a low-frequency electric-quadrupole interaction (EQI) of about 250 Mrad s$^{-1}$, characterized by a small (but nonvanishing) asymmetry parameter. These Fourier transforms also show a broad peak around 900–1000 Mrad s$^{-1}$, which corresponds to a high-frequency EQI char-
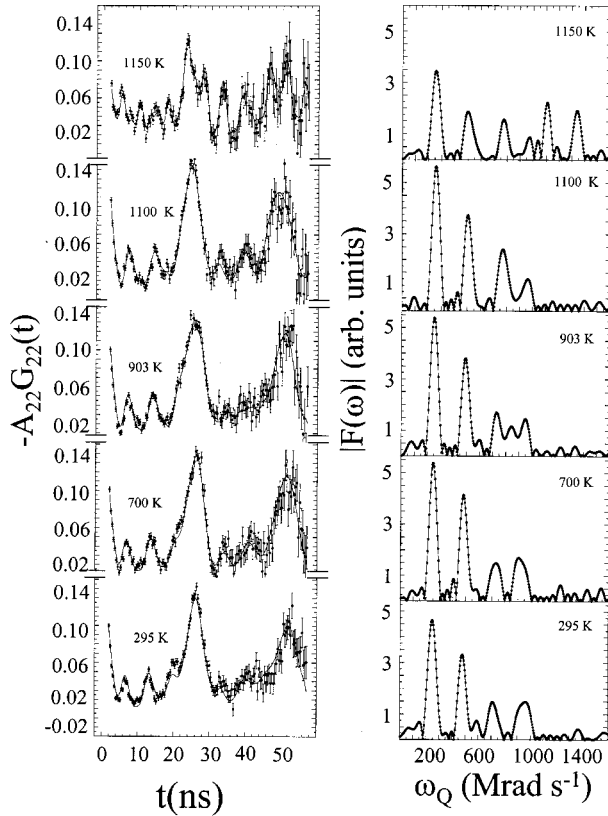
FIG. 2. Perturbation functions and corresponding Fourier transforms measured on a sample of $Zr_3Fe$. For the temperatures from 295 to 1100 K, the Fourier transforms show two well-defined nuclear electric-quadrupole interactions, and sharp spectral lines characterize the perturbation functions. The Fourier transform for 1150 K shows a third interaction (with peaks at approximately 1113 and 1341 $Mrad\,s^{-1}$), which corresponds to a high-temperature phase.

acterized by a high asymmetry parameter of nearly unity. At 298 and 700 K, one broad peak represents $\omega_1$ and $\omega_2$ for this interaction. At 903 K, we see a doublet, as the asymmetry parameter is somewhat lower. At 1100 K, one broad peak includes both $\omega_3$ for the low-frequency interaction and $\omega_1$ for the high-frequency interaction. The single peak to the right represents $\omega_2$ for the high-frequency interaction. These two sets of peaks represent two distinct interactions, which correspond to the two Zr sites in $Zr_3Fe$. For the perturbation function measured at 1150 K, the Fourier transform shows two additional peaks (at approximately 1100 and 1350 $Mrad\,s^{-1}$), which represent an EQI that corresponds to a high-temperature phase and which likely corresponds to the Zr site in $Zr_2Fe$. Upon the decomposition reaction $Zr_3Fe \Rightarrow Zr_2Fe + Zr$, we would expect that Hf probes would occupy four different sites: the two sites for $Zr_3Fe$ (the two frequencies observed as mentioned above), one site for $Zr_2Fe$ (identified with the high-frequency peaks), and one site for the Zr phase (none observed). One possible reason for the absence of the Zr interaction is that the Hf probe in the Zr phase has an associated frequency of approximately 310 $Mrad\,s^{-1}$, which is close to one of the frequencies for the low-frequency interaction for $Zr_3Fe$, so that the peaks corre-

sponding to the Zr interaction could be subsumed under those for the $Zr_3Fe$ interaction. Some line broadening and asymmetry in the peaks for the $Zr_3Fe$ interaction support this explanation. Above 1200 K, the Fourier transforms (not shown) show no discernible interactions (i.e., there are no peaks observed in the perturbation functions), which is consistent with sample melting.

Figure 3 presents a summary of the parameters derived from the fits, which correspond to the two EQI's. As mentioned above, the $Zr_3Fe$ structure has two crystallographically distinct Zr sites, which have a population ratio of 1:2 and which we designate as "site 1" and "site 2," respectively. The observed site-occupancy fractions reflect approximately this ratio. Thus we can identify the high-frequency site with site 1 and the low-frequency site with site 2. For the low-frequency EQI, as the temperature increases, the quadrupole frequency $\omega_Q$ increases slowly and the asymmetry parameter $\eta$ remains relatively constant. For the high-frequency EQI, as the temperature increases, $\omega_Q$ decreases and $\eta$ decreases. For both EQI's, the site-occupancy fractions $f$ remain invariant at $\approx 67\%$ and $\approx 33\%$ over the temperature range corresponding to the single phase of $Zr_3Fe$.

To obtain the EFG components $V_{ij}$ from theory, we carry out nonrelativistic and non-spin-polarized electronic-structure calculations using the first-principles, self-consistent real-space linear muffin-tin atomic sphere approximation (RS-LMTO-ASA) method.[11–13] We calculated the EFG at a Ta nucleus located at both Zr sites in the $Zr_3Fe$ structure (the $^{181}$Hf nuclei decay to excited $^{181}$Ta nuclei, where the EFG is measured). The LMTO is a linear method, and its solutions are valid around a given energy $E_v$, normally chosen at the center of gravity of the occupied part of each $s$, $p$, and $d$ band. We use the von Barth and Hedin parametrization form for the exchange and correlation term of the energy potential.[14] In the LMTO-ASA formalism, space is filled with Wigner-Seitz (WS) spheres centered at all atomic sites. The potential is assumed to have spherical symmetry around each WS sphere. In real space, we work in the orthogonal representation of the LMTO-ASA formalism and expand the orthogonal Hamiltonians in terms of tight-binding parameters. Using the methods described in references above and outlined in the Appendix, we obtain the electronic wave functions from which we calculate the EFG components.

In Table I, we compare the results of the calculations to the measurements. The results of the calculations show that the EFG at a Ta nucleus located on the Zr site 1 is directed parallel to the (001) axis of the crystal, whereas the EFG at a Ta nucleus located on the Zr site 2 is directed parallel to the (001) direction. For both site 1 and site 2, the calculated and measured values of $V_{ZZ}$ are in reasonably good agreement for such a complex calculation. However, the values of the asymmetry parameter $\eta$ differ significantly in both cases. Because we measure the EFG's at Ta nuclei located at Zr sites, some relaxation of the nearest-neighbor atoms relative to Zr may occur. Such relaxation affects the asymmetry parameter $\eta$ (and to a lesser degree the EFG). To test this hypothesis, we performed additional calculations in which we systematically accounted for these relaxations. In the pro-
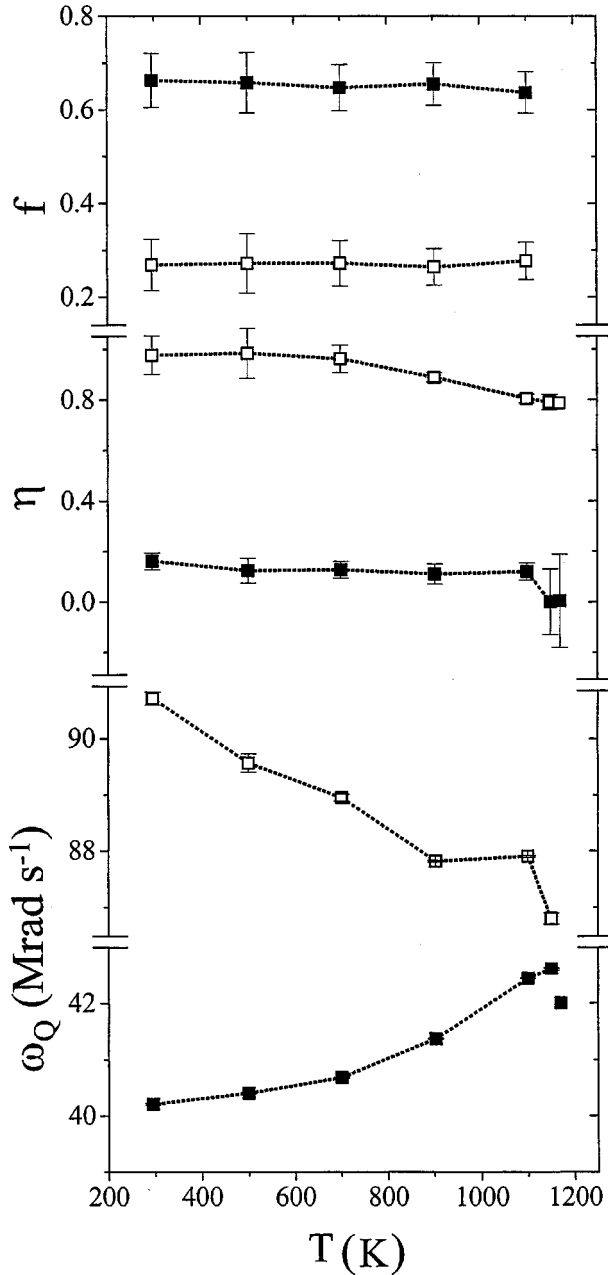
FIG. 3. Summary of the parameters derived from fits of a two-site model to the measured perturbation functions. The site occupancy $f$, the asymmetry parameter $\eta$, and the quadrupole frequency $\omega_Q$ are plotted as a function of temperature, for the two interactions observed, corresponding to the two crystallographically distinct sites. According to the assignment in the text, the values for site 1 are shown in open squares, while those for site 2 are shown in dark squares. The line broadening parameters $\delta_1$ and $\delta_2$ are not shown, as they typically remained at approximately $3 \pm 1 \%$.

totype $Re_3B$ crystal structure of $Zr_3Fe$, the position of the Fe atom is determined by the parameter $y$; in the $Re_3B$ structure, the B atom is at a position $y = 0.744$. Petrilli and Frota-Pessôa determined that, in $Zr_3Fe$, the value of $y$ should be 0.735 to minimize the asymmetry at the Fe site and to reach agreement with EQI's measured using $^{57}$Fe Mössbauer-effect spectroscopy.[15] This value of the $y$ position gives optimal results for the Mössbauer-effect experiments, and it was ob-

TABLE I. Electric-field-gradient parameters $V_{ZZ}$ and $\eta$ for $Zr_3Fe$.

| | $V_{ZZ}$ measured[a,b] ($10^{17}$ V cm$^{-2}$) | $V_{ZZ}$ calculated[c] ($10^{17}$ V cm$^{-2}$) | $\eta$ measured | $\eta$ calculated |
|---|---|---|---|---|
| Zr site 1 | 9.7 | 4.9 | 0.94 | 0.65 |
| Zr site 2 | 4.3 | 6.5 | 0.19 | 1.00 |

[a]Values are calculated from the measured frequencies using $Q = 2.51$ (b) for the electric-quadrupole moment of the $^{181}$Ta spin $I = (5/2)$ intermediate level.
[b]Laboratory temperature values are given.
[c]Calculated values correspond to 0 K, and are for $y = 0.735$.

tained for Fe sites in a crystal having no Hf (Ta) impurities. For site 1, when the first nearest-neighbors (Fe) distance changes to $y = 0.739$ (when Ta is substituted for Zr, the Fe-Ta distance decreases relative to the Fe-Zr distance), while the second nearest neighbors are allowed to relax, the EFG increases to $6 \times 10^{17}$ V/cm$^2$, and the asymmetry parameter increases to 0.95. For site 2, the relaxation of any of the first nine layers of nearest neighbors produces a marked decrease in the value of the asymmetry parameter $\eta$. The agreement cannot be considered quantitative, because we have not found the minimum energy-relaxed structure. However, the current calculations show that, with the appropriate atom positions, we could reproduce the experimental results.

The EFG parameters show distinctly different temperature dependences for site 1 and site 2. For site 1, as Fig. 3 shows, the quadrupole frequency $\omega_Q$ (and consequently $V_{ZZ}$) decreases as the temperature increases, while for site 2, the quadrupole frequency $\omega_Q$ increases. The fact that the quadrupole frequency for one site increases and the quadrupole frequency for the other site decreases could be explained by the different orientations of the principal axes of the EFG for the two sites. Thus this observed difference in temperature dependence would be consistent with a differential thermal expansion, in which the crystal expands more along the (011) direction than along the (001) direction.

## CONCLUSIONS

We have measured the EFG parameters at the two Zr sites in the $Zr_3Fe$ crystal and their temperature dependences, and have compared the values of $V_{ZZ}$ and $\eta$ measured at laboratory temperature to those calculated using the RS-LMTO-ASA method. At temperatures below the peritectic transformation, a two-site model of EQI's in a polycrystalline source provides an accurate representation of the measured hyperfine interactions. Near and above the peritectic transformation, the results show qualitatively the effects of decomposition of $Zr_3Fe$ into Zr and $Zr_2Fe$ and subsequent melting. Overall, the magnitudes of $V_{ZZ}$ and $\eta$ calculated using the RS-LMTO-ASA method agree reasonably well with the experimental values, once we take into account the atomic relaxation induced by the Ta probe.

## ACKNOWLEDGMENTS

## APPENDIX

Theoretically, the EFG at the nucleus is given in terms of a tensor $V_{ij}$ (Ref. 16):

$$V_{ij} = 2 \int^{E_F} \langle \Psi_E | \frac{\partial^2 V(r)}{\partial x_i \partial x_j} | \Psi_E \rangle dE, \qquad (A1)$$

where $|\Psi_E\rangle$ and $V(r)$ are the electronic wave function and the electrostatic potential, respectively, $x_i = x$, $y$, $z$, and $E_F$ is the Fermi energy. The tensor $V_{ij}$ is traceless and symmetric and has in general only five independent components. The $z$ axis is defined along the direction of maximum EFG.

Using the tight-binding approach, the wave functions $|\Psi_E\rangle$ can be expanded in terms of a set of local energy-independent basis functions $|\phi_{m,\mathbf{R}}\rangle$, where $\mathbf{R}$ is a vector position of the site and $m$ indicates the orbital $s$, $p$, or $d$.[17] Then we have

$$|\Psi_E\rangle = \sum_{\mathbf{R}} \sum_{m=1}^{9} a_{m,\mathbf{R}}(E) |\phi_{m,\mathbf{R}}\rangle. \qquad (A2)$$

In Eq. (A2) the coefficients $a_{m,\mathbf{R}}(E)$ are taken to be real.

The tensor $V_{ij}$ is then obtained by neglecting the contributions from local orbitals with $\mathbf{R}' \neq \mathbf{R}$, giving

$$V_{ij} = 2 \sum_{m=1}^{9} \sum_{m'=1}^{9} n_{m,m'} \langle \phi_{m,\mathbf{R}} | \frac{\partial^2 V(r)}{\partial x_i \partial x_j} | \phi_{m',\mathbf{R}'} \rangle, \quad (A3)$$

where

$$n_{m,m'} = \int^{E_F} a^*_{m,\mathbf{R}}(E) a_{m,\mathbf{R}}(E) dE. \qquad (A4)$$

To obtain the components $V_{ij}$, we carry out electronic-structure calculations using the first-principles, self-consistent RS-LMTO-ASA method.[11–13] The LMTO is a linear method, and its solutions are valid around a given energy $E_v$, normally chosen at the center of gravity of the occupied part of each $s$, $p$, and $d$ band. In the LMTO-ASA formalism, space is filled with WS spheres centered at all atomic sites. The potential is assumed to have spherical symmetry around each WS sphere. In real space, we work in the orthogonal representation of the LMTO-ASA formalism and expand the orthogonal Hamiltonians in terms of tight-binding parameters. The eigenvalue problem has then the form

$$(H - E)u = 0,$$

$$\Psi_E = \sum_{RL} [\varphi_{lv}(r_R) + (E - E_v) \dot{\varphi}_{lv}(r_R)] Y_L(\hat{r}_R) u_{RL}(E),$$

$$(A5)$$

where the notation $r_R \equiv |\mathbf{r} - \mathbf{R}|$ was used and where $\hat{r}_R$ is the angle between $\mathbf{R}$ and $\mathbf{r}$. The functions $\varphi_{lv}$ and $\dot{\varphi}_{lv}$ are solutions of a Schrödinger-type equation with quantum number $L = (l, m)$, and their first derivatives with respect to energy, for a spherical potential inside the WS sphere at site $R$, calculated at energy $E_v$. The $Y_L(\hat{r}_R)$ are spherical harmonics and $u_{RL}(E)$ are solutions of the eigenvalue problem.

To obtain $n_{m,m'}$ we use the recursion method.[18] When $m = m'$, $n_m$ is the occupation number per spin associated with the local orbital $m$. In the case of $m \neq m'$, we have to use the off-diagonal terms of the Green functions, which can be calculated using a slightly more complicated procedure.[17]

Using the RS-LMTO-ASA method, according to the equations in Ref. 17, we obtain the tensor $V_{ij}$. Through diagonalization of the $V_{ij}$ matrix, we obtain the components $V_{XX}$, $V_{YY}$, and $V_{ZZ}$ with respect to the principal axes for each site. The largest component of the EFG in magnitude is designated $V_{ZZ}$, and the asymmetry parameter $\eta$ is given by $\eta = (V_{XX} - V_{YY})/V_{ZZ}$, where $|V_{ZZ}| \geq |V_{YY}| \geq |V_{XX}|$.

[1] D. G. Ivey and D. O. Northwood, J. Less-Common Met. **115**, 295 (1986).

[2] C. Lemaignan and A. T. Motta, in *Nuclear Materials*, edited by B. R. T. Frost (VCH, New York, 1994), Vol. 10B, pp. 1–52.

[3] G. L. Catchen, Mater. Res. Soc. Bull. **20**, 37 (1994).

[4] B. Bai and G. S. Collins, in *High-temperature Ordered Intermetallic Alloys VIII*, MRS Symposia Proceedings No. 552 (Materials Research Society, Pittsburgh, 1999), p. 541 and KK.8.7.1-6 (web version).

[5] G. S. Collins, L. S.-J. Peng, and M. Wei, in *High-temperature Ordered Intermetallic Alloys VIII* (Ref. 4), p. 191 and KK.4.2.1-6 (web version).

[6] A. T. Motta, S. E. Cumblidge, G. L. Catchen, R. L. Rasera, A. Paesano, and L. Amaral, Phys. Rev. B **60**, 1188 (1999).

[7] F. Aubertin, U. Gonser, S. J. Campbell, and H.-G. Wagner, Z. Metallkd. **76**, 237 (1985).

[8] A. T. Motta, L. M. Howe, and P. R. Okamoto, J. Nucl. Mater. **205**, 258 (1993).

[9] L. M. Howe, D. Phillips, A. T. Motta, and P. R. Okamoto, Surf. Coat. Technol. **66**, 411 (1994).

[10] A. T. Motta, L. M. Howe, and P. R. Okamoto, J. Nucl. Mater. **270**, 174 (1999).

[11] S. Frota-Pessôa, Phys. Rev. B **46**, 14 570 (1992).

[12] S. B. Legoas, Ph.D. thesis, University of Sao Paulo, Brazil, 1998.

[13] S. B. Legoas and S. Frota-Pessôa, Phys. Rev. B **61**, 12 566 (2000).

[14] V. von Barth and L. Hedin, J. Phys. C **5**, 1629 (1982).

[15] H. M. Petrilli and S. Frota-Pessôa, Phys. Rev. B **44**, 10 493 (1991).

[16] L. Amaral, F. P. Livi, and A. A. Gomes, An. Acad. Bras. Ciênc. **56**, 17 (1984).

[17] H. M. Petrilli and S. Frota-Pessôa, J. Phys.: Condens. Matter **2**, 135 (1990).

[18] R. Haydock, Solid State Phys. **35**, 216 (1980).